LIQUID LIGHT IN CUBIC-QUINTIC NONLINEAR OPTICAL MATERIALS

Humberto Michinel, Maria J. Paz-Alonso, and Jose R. Salgueiro
Area de Optica, Facultade de Ciencias de Ourense, Universidade de Vigo, As Lagoas s/n, Ourense, ES-32005 Spain.

Abstract For a nonlinear optical material with the adequate dependence of the refractive index with light intensity, a condensation phenomenon takes place for a laser beam. This process can be interpreted as a phase transition from a photon gas to a liquid of light. The physical properties of the resulting state, like surface tension, are similar to those of quantum liquids. Here we report a numerical exploration of the dynamics of these light condensates. We show that, as in the case of superfluids, eternal whirpools can be generated in light droplets. We also stress the deep connections and analogies between this new state of matter and Bose-Einstein condensates.

1. Introduction

It was Albert Einstein, during his *miraculous year* 1905 [1], the first to consider seriously the analogies between a beam of light and a gas. By means of statistical mechanics, he calculated the entropy of a monochromatic gas of light quanta, and applied it to explain the photoelectric effect. Thus, if light can be regarded as a gas of photons, a couple of simple questions are: Would it be possible to obtain a liquid of light? What physical properties will it have? The answers are not trivial. In first place, it is known that even in the quantum world the interactions between photons in vacuum are negligible, thus one could expect that photons will not yield to Van der Waals-like interactions. On the other hand, laser photons are a collection of identical non-massive bosons and thus, a liquid of light would have physical properties similar to those of quantum liquids in a Bose-Einstein condensation.

Concerning the first question, it is interesting to consider the effect on the photon gas of an intensity-dependent refractive index[3]. For nonlinear optical materials with a linear growth of the refractive index with light intensity (optical Kerr effect), only in one-dimensional con-

F. Kh. Abdullaev and V. V. Konotop (eds.), Nonlinear Waves: Classical and Quantum Aspects, 327–351.

figurations stable soliton propagation can be achieved. Two and three-dimensional beams, with powers over a critical value, always collapse to a singularity[6]. This behaviour is quite evident if one takes into account that light directs to the regions with higher refractive index due to Fermat's principle. For these materials this zone corresponds to the center of a gaussian laser beam. Thus, if the refractive index shift is strong enough to counteract the natural curvature of the beam, diffraction is overcame and self-focusing takes place.

2. Physical model

Thus, let us begin by remembering some well-known effects concerning non-resonant laser propagation in nonlinear materials. In optical media presenting linear growth of the refractive index shift with light intensity (optical Kerr effect), envelope solitons [2, 3, 4] can be produced for one-dimensional propagation. They can be obtained as pulses in optical fibers with anomalous dispersion (temporal solitons) or continuous beams in several planar configurations. On the other hand, wild unstable phenomena like blow-up and catastrophic self-focusing take place for intense two-dimensional propagation in bulk Kerr-like materials[5, 6]. However, collapse can be limited if the nonlinear growth of the refractive index saturates for high powers, and thus, stable two-dimensional stationary beams can be obtained [7, 8].

In the present work, we will analyze the dynamical properties of laser beams and pulses propagating through a nonlinear optical material with the following refractive index:

$$n(I) = n_0 + n_2 I - n_4 I^2. \tag{1}$$

Where n_0, n_2 and n_4 are positive constants determining the nonlinear response of the optical material with the intensity (I) of the light beam. This kind of refractive index represents the so-called cubic-quintic optical materials [9, 10, 11, 12, 13, 41] and it can be considered as a Taylor expansion up to I^2 terms of more complicated optical nonlinearities. The above $n(I)$ grows with I for low powers, and diminishes for high powers due to the contribution of the negative $n_4 I^2$ term. A very interesting example of materials which correspond to the previous refractive index are the recently reported nonlinearities of chalcogenide glasses[14], which show an intensity-dependent refractive index that can de fitted by Eq. (1). Our aim in the present paper, will be to show that this change in the sign of the nonlinear response with the intensity, yields to the formation of light condensates with physical properties resembling those of fluids. This light condensates can be obtained as well as continuous or pulsed

beams. Thus, we will use respectively the terms *light streams* or *light drops*, to refer to each case.

We will analyze in first place the propagation along z, in the paraxial regime, of a continuous linearly-polarized laser beam trough a nonlinar optical material with the above refractive index $n(I)$. The dynamics of the envelope of the electromagnetic wave $\Psi(x, y, z)$ is given by a generalized Non Linear Schrdinger Equation (NLSE) of the form[9]:

$$2ikn_0\frac{\partial\Psi}{\partial z} + \nabla_\perp^2\Psi + 2k^2n_0\left(n_2|\Psi|^2 - n_4|\Psi|^4\right)\Psi = 0, \tag{2}$$

where $k = 2\pi/\lambda$ is the wavenumber in vacuum and $\nabla_\perp^2 = \partial^2/\partial x^2 + \partial^2/\partial y^2$ is the transverse Laplacian operator. The previous equation can be interpreted in the light of results obtained for gaseous Bose-Eintein condensates (BEC) where it is called a Gross-Pitaevskii Equation (GPE). In the GPE, the term $\nabla^2\Psi$ represents the kinetic energy that tends to broad the atom gas. The analogous to the optical nonlinearity is the scattering length, which determines whether the interactions between atoms will be attractive (self-focusing) or repulsive (self-defocusing). Thus, a term in the GPE that counteracts the motion of the atoms may be considered as a cooling term. Therefore, coming back to the NLSE, we can conclude that *an optical material with self-focusing nonlinearity acts as a cooling medium for a photon gas.* The key point is that it is neccessary to saturate the growth of the nonlinear shift in order to avoid the collapse of the beam envelope to a singularity. This happens in materials with the cubic-quintic nonlinearity.

Typical values of the above parameters can be chosen to fit usual experimental configurations by taking: $n_0 = 1.8$, $n_2 \approx 2 \cdot 10^{-4} cm^2/GW$ and $n_4 \approx 2 \cdot 10^{-3} cm^4/W^2$, with $\lambda = 1600nm$. Thus, nonlinear effects become significant for values of I in the range of GW/cm^2. The physical picture of the above nonlinearity is evident: for low intensities, propagation remains in a quasi-linear regime. If the power is increased, nonlinear self-focusing tends to counteract diffraction and will overcome it for a critical beam flux. This would yield to blow-up in pure Kerr materials ($n_4 = 0$). However, for high powers, the defocusing effect of the term $n_4 I^2$ will balance collapse, yielding to a stable two-dimensional beam. Thus, for an adequate power, a beam traversing such a nonlinear optical material will yield to a compact state in which light acquires surface tension properties, like droplets of usual liquids.

3. Stationary nodeless states

Before analysing the dynamics of laser beams, it is useful to take a look to the spatial profile of the lowest-order stationary solutions of Eq.

(2), which are nodeless wavefunctions of the form: $\Psi = \psi(r)e^{i\beta z}$, where β is the nonlinear phase shift (propagation constant) and $\Psi(\infty) = 0$. It can be seen in Fig. 1 that the shape and properties of the above states depend crucially on the value of β. To the contrary of linear waveguides (where there is only one fundamental mode with a given β) nonlinear propagation yields to a continuum of nodeless eigenstates. This is evident, as the nonlinear beam generates its own waveguide during propagation. Thus, we have found by numerical integration, the stationary states corresponding to Eq. (2) for increasing values of the nonlinear phase shift, starting from $\beta = 0$. The result is a continuum of stationary states with different shapes and increasing values of the beam power $N = \int |\Psi|^2 dxdy$. Some of these spatial profiles are shown in the insets of Fig. 1.

The form of the stationary solutions of Eq. (2) has been analysed by several authors[15, 16, 17]. It is well known, for instance, that there is a minimum power threshold N_0 to generate a stationary beam. Obviously, this minimum beam flux coincides with the collapse power threshold for a gaussian beam in a bulk Kerr media[18, 19]. We must also point that there is a critical value β_c of the propagation constant for which N diverges. Thus, for $\beta > \beta_c$, no stationary solutions can be obtained. Although there are good analytical approximations for shapes of the previous stationary beams[17], less attention has been paid to investigate the peculiar form of the spatial profiles of Fig. 1 from a physical point of view. Thus, let us try to extract a qualitative picture of the properties of the mentioned stationary beams, by analyzing the changes in the shape of the eigenstates of Eq. (2) for growing values of β.

As it can be appreciated in Fig. 1, low values of the beam flux N (i.e.: $\beta \to 0$) yield to light distributions with quasi-gaussian profiles. Note that the intensity scale in the inset a) is different and thus the corresponding profile is smoother than those in b) and c). As β is incremented, the beam flux grows and the spatial shapes tend to narrow, keeping approximately the gaussian shape and reaches a minimum width and a maximum peak for an intermediate power. For larger values of β, the beam flux grows rapidly and the peak intensity of the light distribution saturates due to the effect of n_4. The light distributions tend to supergaussian profiles and thus, *high power stationary beams yield to wide top flatted profiles ended by sharp decays*. Moreover, as the sharp ends of intense beams are very similar, we can conclude that the shapes of high power beams differ only on the length of the top flat.

Thus, let us reconsider the previous scenario in the light of statistical mechanics of a "photon gas". The situation looks as follows: low powers (i.e.: $\beta \to 0$ quasi-linear regime) yield to smooth gaussian-like spatial

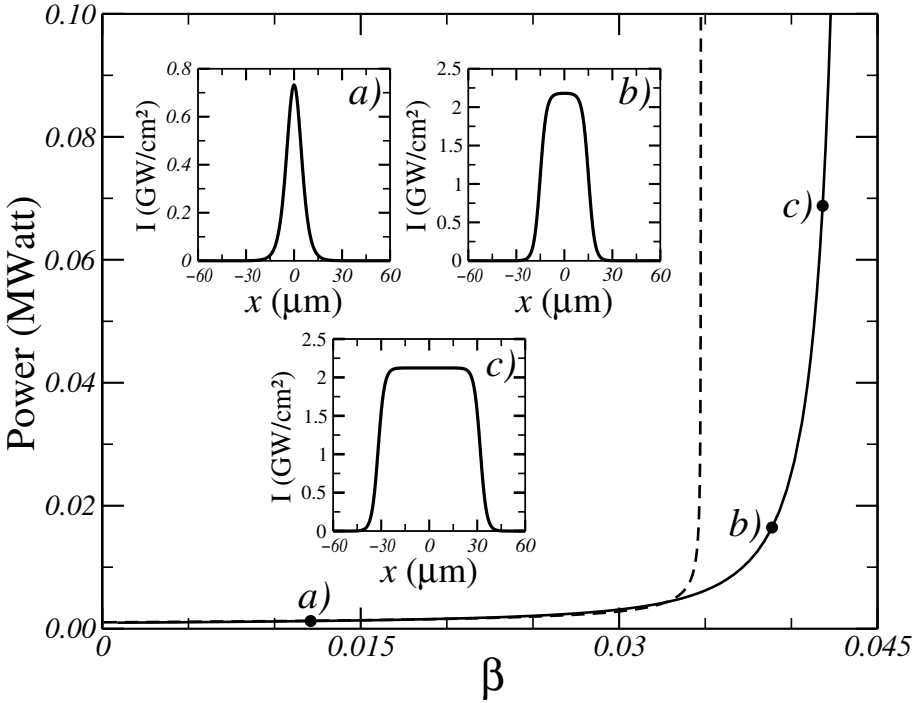

Figure 1. Beam power (N) vs nonlinear phase shift (β)for stationary nodeless states. Solid line: numerical; dashed line: variational. Note that N grows monotonically with β and the gap at $\beta = 0$. Insets: beam shapes corresponding to several powers. Note that the intensity scale in a) is different.

distributions of the "photon gas" and the dominant contribution in Eq. (2) is diffraction ($\nabla^2\psi$) that can be interpreted as a kinetic term (expansion of the photon gas). For stationary beams with higher powers, the Kerr self-focusing term given by n_2, becomes significant and tends to narrow the shape of the light distribution. The beam would collapse for powers over a critical value; however, the defocusing effect of n_4 dominates for high powers and avoids blow-up. The comparison between the low and high power spatial profiles resembles the density distributions of particles inside a gas for low values of N, (smooth quasi-gaussian spatial distribution, representing high delocalization) or a condensed supergaussian shape for high powers (almost constant photon density inside the beam and sharp decay at the boundary). The analogy makes more sense if the nonlinear material is regarded as a "cool region" where the kinetic term $\nabla^2\psi$ of Eq. (2) is balanced by nonlinear effects. Stable "light streams" are formed due to competing effects of diffraction, the Kerr term (n_2) and the self-defocusing nonlinearity (n_4) , in a similar way as Van der Vaals forces form liquid droplets in a gas-liquid condensation. The analogy is more evident in the case of pulsed beams, where "light droplets" will be obtained. We will analyze this case in the last section of the present work.

Thus, if one assumes the previous picture, the following step is to formulate ideal experiments to detect typical properties of liquids in the mentioned liquid light states, like the existence of surface tension properties.

4. Dynamics of collective oscillations

To get a deeper physical insight in the properties of the above light distributions, we have performed a variational analysis of the frequency spectrum of the small amplitude oscillations of slightly perturbed stationary beams. The perturbation can be experimentally implemented with a thin lens, that adds a slight curvature to an input gaussian beam. Thus, we can model the evolution by means of the following trial function:

$$\Psi(r,z) = \psi(z) e^{\left[-\frac{r^2}{2w^2(z)} + ib(z)r^2\right]}, \tag{3}$$

where ψ, w and b are quantities depending on z, corresponding to the peak amplitude, beam width and curvature, respectively. Following the standard variational procedure[42, 15, 16], after minimization of the corresponding Lagrangian density over the set of trial functions from Eq. (3), an ordinary newton-like differential equation is obtained for the above parameter w. These equations can be reformulated in terms of

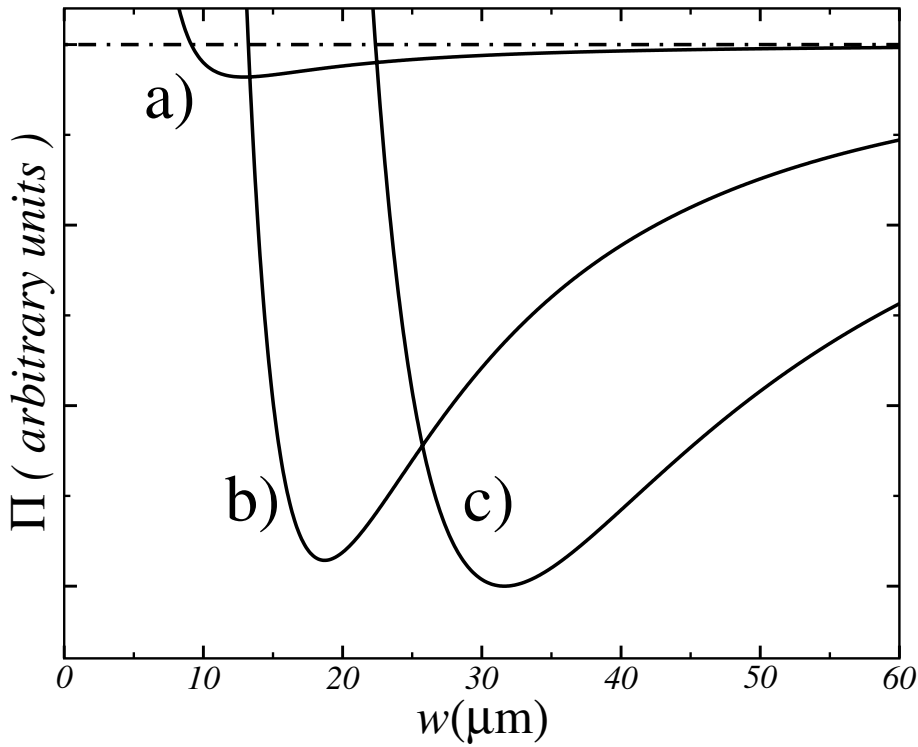

Figure 2. Potential functions given by Eq. 4 of the nodeless states a), b) and c) from Fig. 1 .

effective potentials for equivalent particles in the following form:

$$\Pi = \left(\frac{1}{k^2 n_0^2} - \frac{n_2 N}{2\pi n_0}\right) w^{-2} + \frac{2n_4 N^2}{9\pi^2 n_0} w^{-4}, \tag{4}$$

In Fig. 2, we have plotted the shape of the previous potentials for three different values of the peak power, corresponding to the shapes of the insets in Fig. 1. As it can be seen in the caption, the higher N, the depper Π. The minimum width of the potential is achieved for the b) eigenstate. The widths of the perturbed beams will evolve oscillating around the minimum of Π, as classical particles in potential wells, playing z the role of time. The variational analysis, although not exact, provide the widths of the stationary states w_s, as function of the beam power. They are given as the values of w for which Π is minimum. From a simple inspection of Eq. (4) it is obtained the following value for the width of the beam:

$$w_s^2 = \frac{8n_4}{9n_2} \frac{N^2}{N - N_0},$$

where N_0 is the following critical value for the beam flux:

$$N_0 = \frac{2\pi}{k^2 n_0 n_2}, \tag{5}$$

The value of N is the small gap of the beam power at $\beta = 0$ of Fig. 1. It is straightforward to calculate the minimum width w_m of a stationary beam, which is achieved for $N = 2N_0$ and is given by $w_m = \frac{8}{3k_0 n_2}\sqrt{\frac{\pi n_4}{n_0}}$. For the experimental values given above, it is easily obtained that $w_m \approx 6.4\mu m$, which yields to peak powers in the range of $2GWcm^2$ to generate the stationary states. Thus, the variational model predicts a minimum beam power to generate the stationary states that we calculated above numerically. Obviously, Eq. (5) coincide with the critical collapse threshold for a gaussian beam in a bulk Kerr material [19]. The comparison with direct numerical calculations, as it can be appreciated in Fig. 1, yields to a very good agreement (error below 1%) for low values of β. However, it must be stressed that, as the shape of the stationary states deviates from the gaussian profile, the fit of the theoretical and the numerical curves is only qualitative.

In second place, notice that expanding Π around its minimum, it is possible to obtain the frequencies ν of small amplitude oscillations along z of perturbed stationary states, as functions of the main parameters involved. To get a more physical view of the light condensates, it is interesting to consider ν as a measure of the "rigidity" of the different stationary states. After a trivial Taylor expansion around the minimum of Π, it is obtained:

$$\nu = \frac{9\pi}{4\sqrt{2}k^3 n_0^2 n_4} \frac{\left(\frac{N}{N_0} - 1\right)^{\frac{3}{2}}}{N^2}, \tag{6}$$

As it can be seen in Fig. 3, the variational analysis reveals that a maximum rigidity of the light condensate is achieved for a given value of N (or equivalently β). The critical value of N corresponding to the maximum frequency can be easily calculated by taking $d\nu/dN = 0$, and is given by:

$$N_{cr} = \frac{8\pi}{k^2 n_0 n_2} = 4N_0, \tag{7}$$

In Fig.3, we can observe that the variational method has only a qualitative agreement with the numerical (solid line) calculation. From the shape of the cuves, we can argue that N_{cr} is the critical value over which the surface tension properties of the light beams appear. The reason is that the maximum in the frequency ν_{max} acts as a gap for the excitation

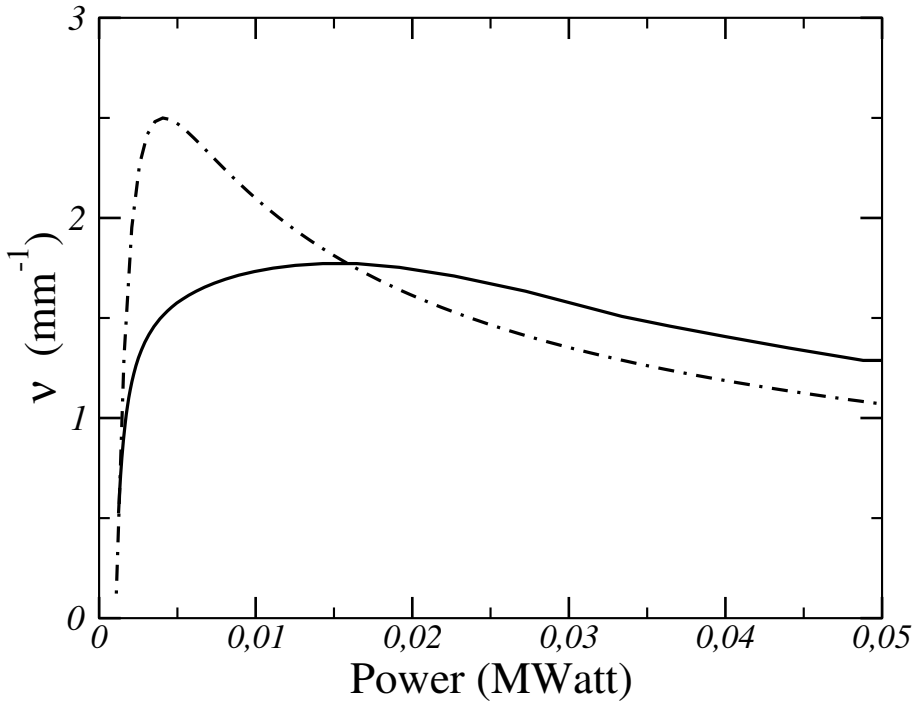

Figure 3. Resonance frequencies (ν) of the nodeless states as a function of the beam power. Dashed (solid) lines correspond to variational (numerical) calculations, as given by Eq. (6).

of linear waves from the stationary state, and thus radiation is blocked for beams with $\nu > \nu_{max}$.

5. Collisional dynamics

In the present section we analyse numerically, the propagation of a light condensates through a bulk cubic-quintic nonlinear optical material in the presence of boundary conditions and localized inhomogeneities (holes). The propagation equation for the above waveguide in the paraxial regime is a generalized NLSE, including the effect of boundaries or holes. The experimental parameters are in the same range as in the previous sections.

Our computer simulations show that there is a deep analogy between incompressible fluid dynamics and interference behavior of light condensates at boundaries and localized discontinuities. This can be understood thinking of light condensates as having some kind of "surface tension", analogous to that of a liquid droplet. Considering that diffraction in

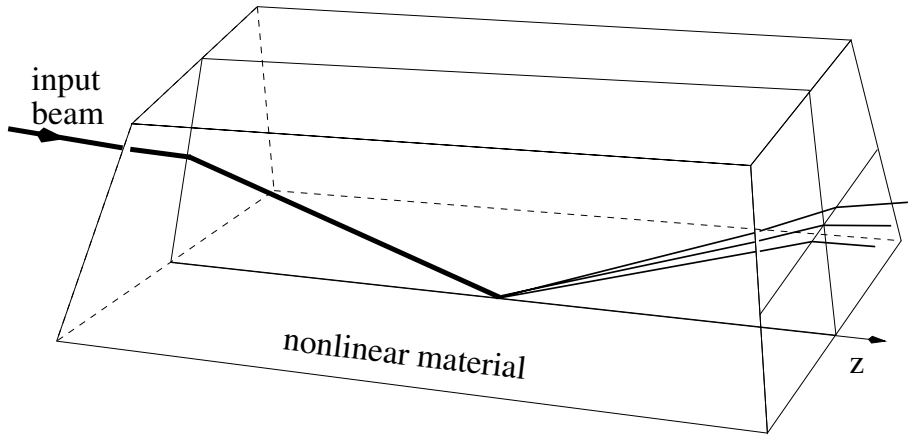

Figure 4. Sketch of the numerical simulation of Fig. 5, showing total reflection at a nonlinear-linear interface.

the NLSE plays the role of a kinetic energy term, a Kerr-like material can be regarded as a "cold medium" that tends to compress the photon gas (i.e.: beam self-focusing). From this point of view, when collapse is stopped due to quintic defocusing terms, the situation is similar to droplet condensation due to Van der Vaals forces.

As in the case of liquids, one can expect surface tension properties from the resulting light condensates. To show this, we present two particular cases from our numerical investigation. Both simulations correspond to a radial stationary fundamental state of the propagation equation. The beam is $25\mu m$ width and its peak intensity is $2.0GW/cm^2$. The numerical simulations has been performed with standard Fourier beam propagation method in a 1024 points grid. In Fig. 4, we show a sketch of the numerical calculations of Fig. 5, where we have simulated internal reflection inside a bulk cubic-quintic material surrounded by air. The interference pattern when the beam reaches the boundary, clearly resembles crushing of a liquid drop thrown towards a solid wall which splits into smaller droplets. We have performed large series of numerical explorations for different angles of incidence, from quasi-elastic to complete inelastic range. Showing that surface tension effect provides the beam a high stability.

In Fig. 6 we have plotted a collision with a $8\mu m$ air hole immersed in the bulk nonlinear material. The role of the surface tension is evident: the beam is strangulated when it intersects the hole. However, it recovers its original form if the angle of incidence is below a critical value. Both simulations show that light condensates behave against collisonal perturbations in a similar fashion as liquids. The raising of surface

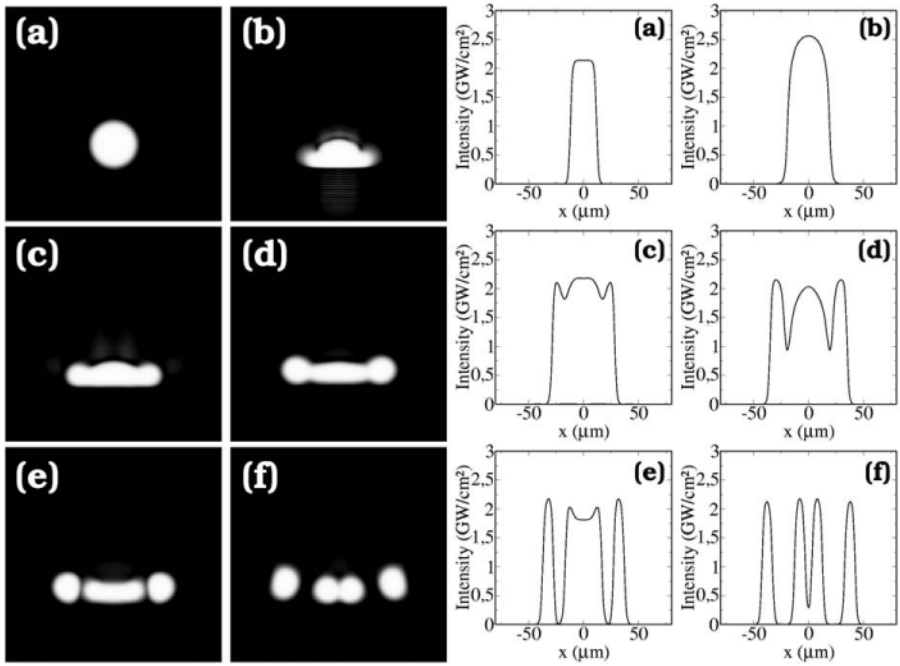

Figure 5. Numerical simulation corresponding to the sketch of 4. Left: grascale images of the transverse xy plane for a) $z = -10$, b) $z = 0$, c) $z = 10$, e) $z = 20$ and f) $z = 40$ (in μm). Right: Maximum intensity profiles along the x axis corresponding to the left images. The scale of the x axis is the same in all the pictures.

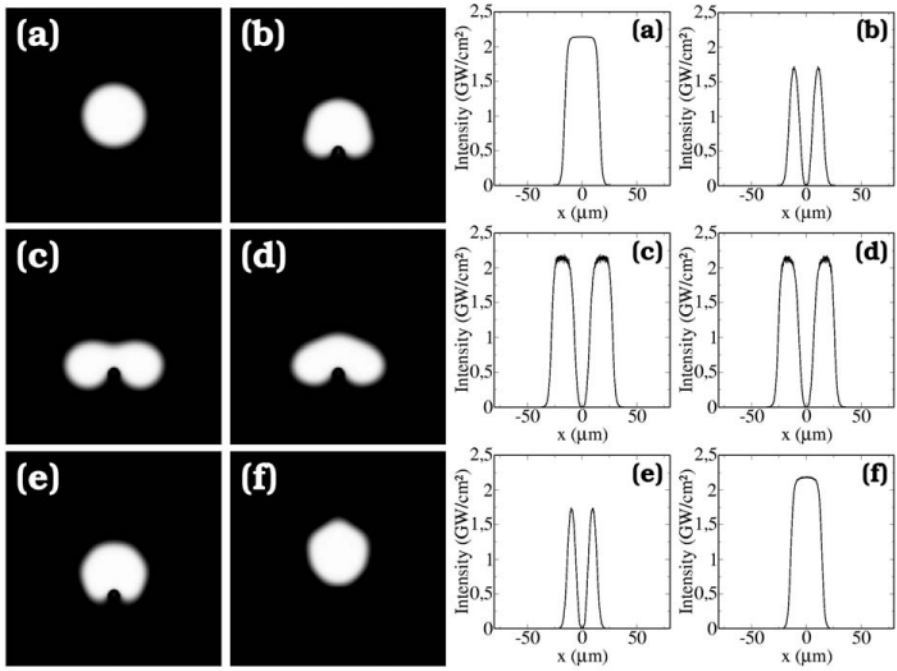

Figure 6. The same as Fig.5 for total reflection at an $8\mu m$ air hole.

tension properties can be qualitatively explained as a balance between the radiation pressure inside and outside the beam. Inside the beam, the refractive index is greater than outside, due to the nonlinear effects. However, a detailed understanding of the phenomenon should start from a thermodynamical point of view, defining quantitative concepts as the temperature and entropy of the beams for a given nonlinearity. This is a deep problem that we address to further research.

6. Pulsed Beams

If the beam is pulsed, time must be included in the simulations. Thus, an extra second derivative with respect to "proper time" should be added to Eq. (2) in order to take into account the effect of second-order dispersion. The corresponding NLSE, becomes 1+3 dimensional, and extra difficulties are added to the numerical simulations. Not only the increase in the length of the calculations is an inconvenient but also the representation of the data obtained. The need for analytical tools as the variational model is more evident in this case.

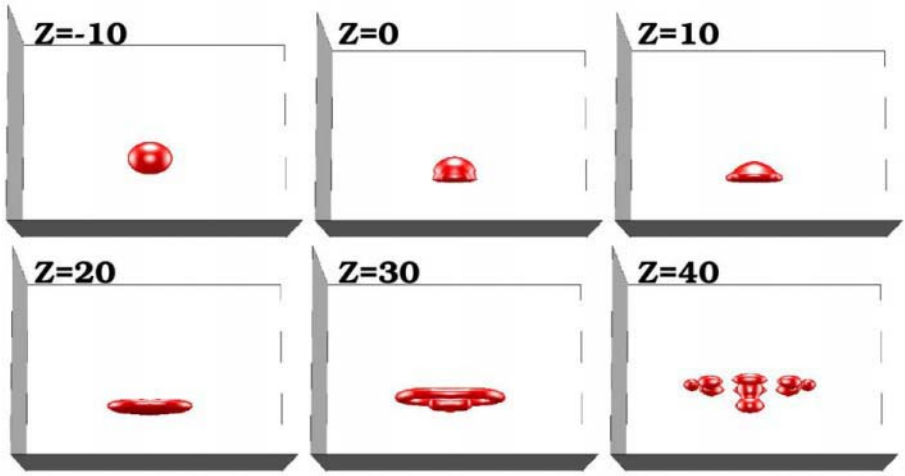

Figure 7. Numerical simulation of the collision of a light drop against a planar boundary (not visible in the graphs). The values of z in each picture are the distances from the center of the pulse to the origin of coordinates. The paper plane is xy and z is perpendicular to the paper plane. The experimental parameters are given in the text.

Thus, taking into account the data obtained for the 2-dimensional case of laser beams, we will analyze the properties of pulsed beams, which propagate in cubic-quintic materials, corresponding to the same material parameters of Fig. 5. The result is plotted in Fig. 7, where it can be seen that the effect of the planar boundary between the non-linear and the linear material (not shown in the captions) is to generate a corona of droplets in a similar fashion as it happens in the crushing of a liquid drop. In fact, the dominant effect in the generation of smaller pulses at the boundary is modulational instability[8, 20] around the rings formed by diffraction.

We must notice the deep connection of this case with the dynamics of Bose-Einstein Condensates (BEC) in alkalii gases. In fact, the collective dynamics of a BEC in the absence of a trapping potential, is given by a NLSE. If three-body elastic interactions are present, the equation for the coherent cloud includes a quintic nonlinear term as in Eq. (2). Thus, it is evident that similar behaviour as shown in Fig. 7 could be expected for BECs with the adequate experimental configuration. In fact, the possibility of gas-liquid phase transitions in Bose Eintein condensates has been recently put forward by several authors[21].

7. Light whirlpools

In wave mechanics, a vortex is a screw phase dislocation, or defect [22] where the amplitude of the field vanishes. The phase around the singularity has an integer number of windings, l, which plays the role of an angular momentum. For fields with non-vanishing boundary conditions, this number is a conserved quantity and governs the interactions between vortices as if they were endowed with electrostatic charges [23]. Thus, l is usually called the "topological charge" of the defect.

Vortices are present in very different branches of physics like fluid mechanics, superconductivity, Bose-Einstein condensation, astrophysics or laser dynamics, among others [24]. In optics, a vortex with charge l takes the form of a black spot surrounded by a light distribution. Around the dark hole, the phase varies from zero to $2l\pi$. This defects appear spontaneously in light propagation through turbulent media and can also be produced by appropriately shining a computer generated hologram [25, 26]. The trace of vortices in a light field is a characteristic "fork-pattern" interferogram produced by superposition with a tilted planar wave. The first experimental works on optical wavefront dislocations were carried out in the 80's, in the context of adaptive systems, where phase singularities were a severe problem for image reconstruction techniques [27, 28]. Since then, they have been studied, among other fields, in optical tweezing [29], particle trapping [30], laser cavities [31], optical interconnectors [32] or even to perform N-bit quantum computers [33].

Concerning light vortices in the nonlinear regime [34], the first theoretical works analysed their stability in Gaussian-like distributions propagating in optical Kerr materials [35]. It was found for a cubic self-focusing refractive index, that a beam of finite size will always filament under the action of a phase dislocation. This also stands for saturable self-focusing nonlinearities. On the other hand, vortex states were predicted and found experimentally for self-defocussing materials both in the Kerr case for continuous background [37] and in the saturable case with finite size beams [39].

It was shown in [15, 38] that stable vortex states with $l = 1$ can be obtained as stationary states of the propagation of a laser beam through cubic-quintic optical materials[9]. This kind of nonlinearity is characterized by the $\chi^{(3)} > 0$ and $\chi^{(5)} < 0$ components of the nonlinear optical susceptibility and changes from self-focusing to self-defocussing at a given intensity[40]. It has been recently shown that a gas-liquid phase transition takes place in light beams propagating in this type of materials[41].

In the next sections we will show that stable vortex states with arbitrary value of the angular momentum exist and its peak amplitude and propagation constant tend asymptotically to values that do not depend on l as the beam flux is increased.

8. Azimuthal eigenstates

For Eq. (2) we have calculated the azimuthal stationary states of the form: $\Psi(r,\theta,z) = \psi(r)e^{i(\beta z + l\theta)}$. The quantity β is the nonlinear phase shift or propagation constant. For a given integer value of l, a continuum of eigenstates can be obtained with β varying between zero and a critical value β_{cr} over which no stationary states can be found[15]. The profiles of the eigenstates for several values of l and β are plotted in Fig. 8. We particularly show states with $l = 3$ and $l = 4$ since these are the first values of l for which all the eigenstates were previously found unstable, as well as two examples of huge angular momentum states ($l = 10$ and $l = 50$). It can be appreciated in the graphs that values of β below $0.5\beta_{cr}$ yield to light distributions with smooth and wide Gaussian-like shapes. As β is incremented, the beam flux grows and the spatial profiles narrow, yielding to a minimum thickness of the ring of the stationary state, for values of β around $0.8\beta_{cr}$ keeping approximately the Gaussian shape. For larger values of β, the beam flux grows rapidly with β and the peak amplitude of the light distribution saturates due to the effect of n_4, reaching asymptotically the value A_{cr}, which is slightly below the maximum amplitude. Thus, high power beams show spatial light distributions with flatted tops in their profiles, similar to those of hyper-Gaussian functions[17] as in the case of nodeless beams.

It also worths to mention that the central hole increases its size with the topological charge, as it can be seen comparing the profiles for $l = 3, 4$ with $l = 10$, 50. However, as the value of β approaches a critical value, the thickness of the external ring grows faster than the internal hole and thus, the final result takes always the asymptotic form of a dark spot surrounded by a larger ring of light of almost constant shape which ends abruptly at a given radius. Close to the origin the profiles follow the linear regime with $\psi \propto r^l$.

Another intriguing fact is that both β_{cr} and A_{cr} do not depend on the value of the topological charge. This is shown in Fig. 9, where the peak value of the intensity has been plotted as a function of β. As it can be appreciated, whatever the value of l all the curves join at the same point. In the inset, it can be seen a detail of the critical zone. This means that the critical value of the propagation constant only depends on the nonlinearity and not on the value of l. Thus, we can deduce

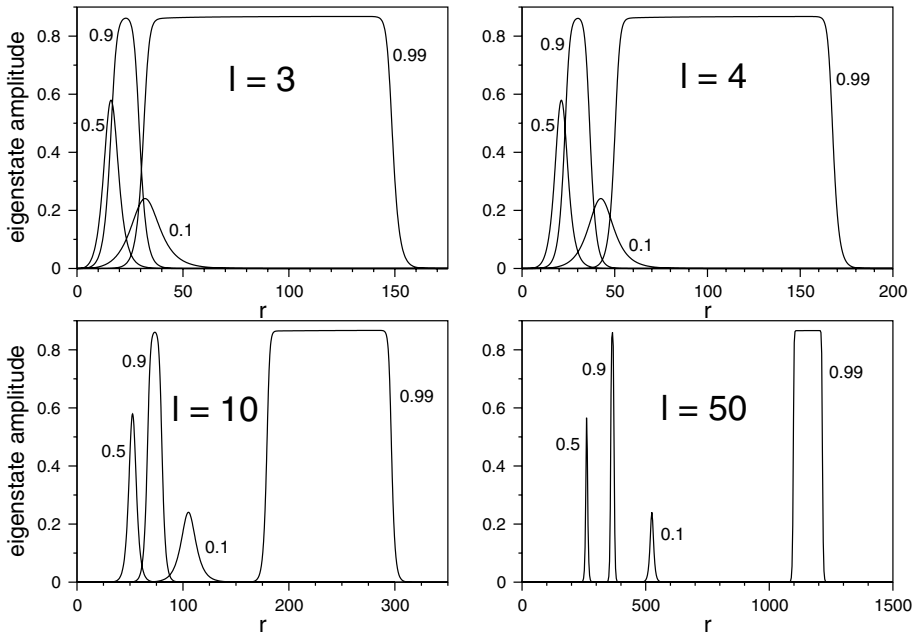

Figure 8. Numerically calculated radial amplitude profiles of the stationary azimuthal states of Eq. (2) for $l = 3, 4, 10$ and 50 with β/β_{cr}=0.1, 0.5, 0.9 and 0.99. We have used a relaxation method and a normalised equation with $n_2 = n_4 = k = 1$, $n_0 = 1/2$.

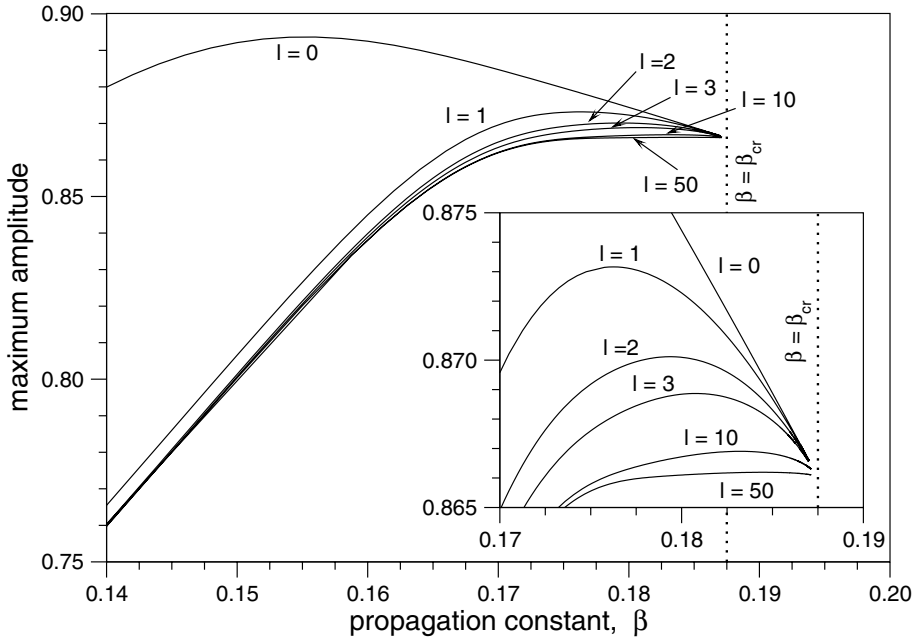

Figure 9. Eigenstates maximum amplitude vs propagation constant for angular momenta l=0, 1, 2, 3, 10 and 50. All the curves join at the point $A = A_{cr} = 0.866$, $\beta = \beta_{cr} = 0.1875$. Inset: detail of the zone close to β_{cr} where the calculations become delicate. The normalisation is the same as in Fig. 8.

that spinning solitons are composite objects: one part is the top-flatted background and the other is the vortex core.

To explain the properties of the above light distributions, we have performed a variational analysis[17] by means of the square-like trial function:

$$\Psi_v(r, \theta, z) = \psi_v(r) \exp[i(\beta z + l\theta)],$$

where $|\psi_v|^2$ takes the constant value $|A|^2$ inside the interval $[(r_0 - w/2), (r_0 + w/2)]$, and zero elsewhere, being w the mean radius of the light ring. As it can be appreciated by comparison with Fig. (8), this square-shaped function is very adequate for the region close to β_{cr}, where the profiles of the stationary states become almost square. Using this trial function and performing the usual average[42] over the lagrangian density associated to Eq.(2), the following relationships are obtained[15]:

$$\beta = k \left(\frac{n_2}{2} |A|^2 - \frac{n_4}{3} |A|^4 \right); \tag{8}$$

$$\left[\beta - k\left(n_2|A|^2 - n_4|A|^4\right)\right] = \frac{l^2}{kn_0}\left(\frac{w^2}{6} + 2r_0^2\right)^{-1}, \tag{9}$$

and thus, in the limit $w, r_0 \to \infty$ the last term of the above equation vanishes and it is obtained the critial value of the amplitude A_{cr}:

$$|A_{cr}|^2 = \frac{3}{4}\frac{n_2}{n_4}, \tag{10}$$

corresponding to $\beta = \beta_{cr} = 3kn_2^2/16n_4$. The comparison of these analytical results with the numerical calculations shows an excellent agreement. Taking the normalised form of Eq. (2), making $n_2 = n_4 = k = 1$ and $n_0 = 1/2$, it is obtained that $\beta_{cr} = 0.1875$ and $A_{cr} = 0.866$, which are exactly the values obtained numerically, as it can be seen in the inset of Fig. (9). This good result is due to the choice of the trial function, which fits very accurately with the exact numerical solution for values close to the critical point.

9. Stability analysis of the azimuthal eigenstates

In order to test the stability of the stationary states, we calculated the growth rates of small azimuthal perturbations to find out the value of β at which they vanish. Additionally, in order to asses the accuracy of the previous analysis, we propagated some eigenstates with a split-step Fourier method and measured the distances at which the unstable states split. The inverse of these values should coincide, except for a constant scale factor, with the dominant perturbation eigenvalues calculated in the azimuthal instability analysis. Finally, we have also simulated other kind of perturbations like total reflection at the boundary between a cubic-quintic material and air. As we will see below, the eigenstates show robust behaviour against these collisions and preserve their angular momentum although strong oscillations are observed.

To carry out the perturbation analysis we add to the original eigenstate a small p-order azimuthal perturbation function[43]:

$$\Psi(r,\theta,z) = [\psi(r) + f(r)e^{\delta_p z + ip\theta} + h(r)e^{\delta_p^* z - ip\theta}]e^{i(l\theta+\beta z)}, \tag{11}$$

where $f(r) = f_1(r) + if_2(r)$ and $h(r) = h_1(r) + ih_2(r)$ are the complex components of the eigenstate of the p-order azimuthal perturbation and δ_p is the corresponding perturbation eigenvalue. In this way, the real part of δ_p constitutes the growth rate of this perturbation. Substitution of this perturbed eigenstate in Eq. (2) leads to the following set of coupled differential equations:

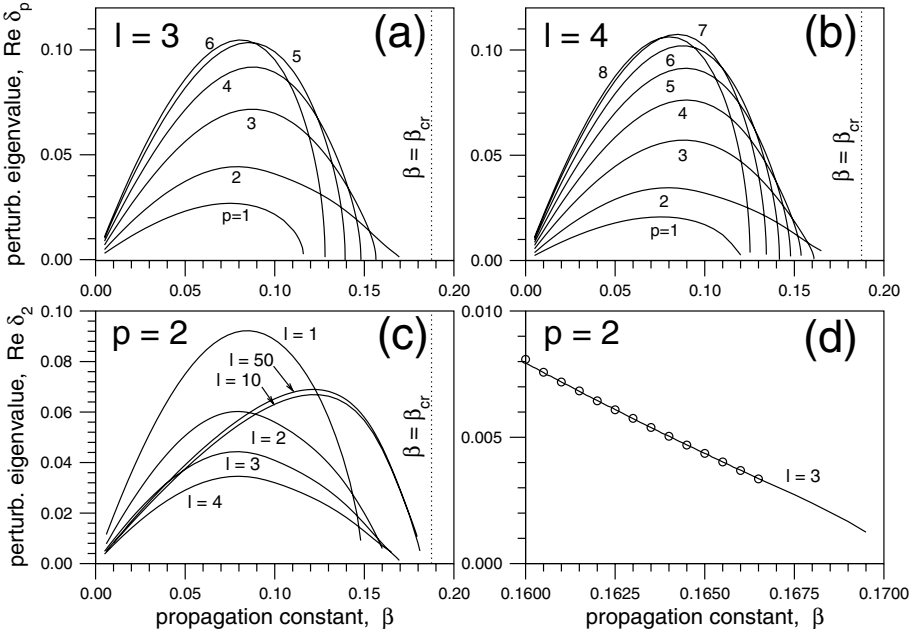

Figure 10. Growth rate of the azimuthal perturbation vs β. In (a) and (b), the angular momentun is fixed (l=3 for (a), l =4 for (b)) and the values of the perturbation order p are indicated by labels near the curves. In (c) the growth rate for the perturbations with p=2 for l=1, 2, 3, 4, 10 and 50 are plotted. In (d), a comparison between the inverse of the splitting distance (dots) and $p = 2$ perturbation eigenvalue for unstable states with $l = 3$ is shown.

$$i\delta_p f + \nabla^2_{rr} f - \frac{(l+p)^2}{r^2} f + Q(\psi) f + R(\psi) h^* = 0 \tag{12a}$$

$$i\delta_p h + \nabla^2_{rr} h - \frac{(l-p)^2}{r^2} h + Q(\psi) h + R(\psi) f^* = 0, \tag{12b}$$

where $\nabla^2_{rr} \equiv \partial^2/\partial r^2 + (1/r)\partial/\partial r$, $Q(\psi) \equiv -\beta + (2 - 3|\psi|^2)|\psi|^2$ and $R(\psi) \equiv (1 - 2|\psi|^2)|\psi|^2$. The solution of this equation system using a Crank-Nicolson propagation scheme [43] yields to the growth rates for different order perturbations versus propagation constant.

The results are illustrated in Fig. (10). Figs. 10(a)-(b) show the growth rates for vortices with angular momentum $l = 3$ and $l = 4$. The maximum growth rate corresponds to perturbation eigenvalues with $p \approx 2l$, while perturbation $l = 2$ has been proved to be the most persistent (the one which remains till highest values of β before vanishing) despite the value of the angular momentum. Hence, in Fig. 10(c) we plot the curve associated to this perturbation for different values of the angular

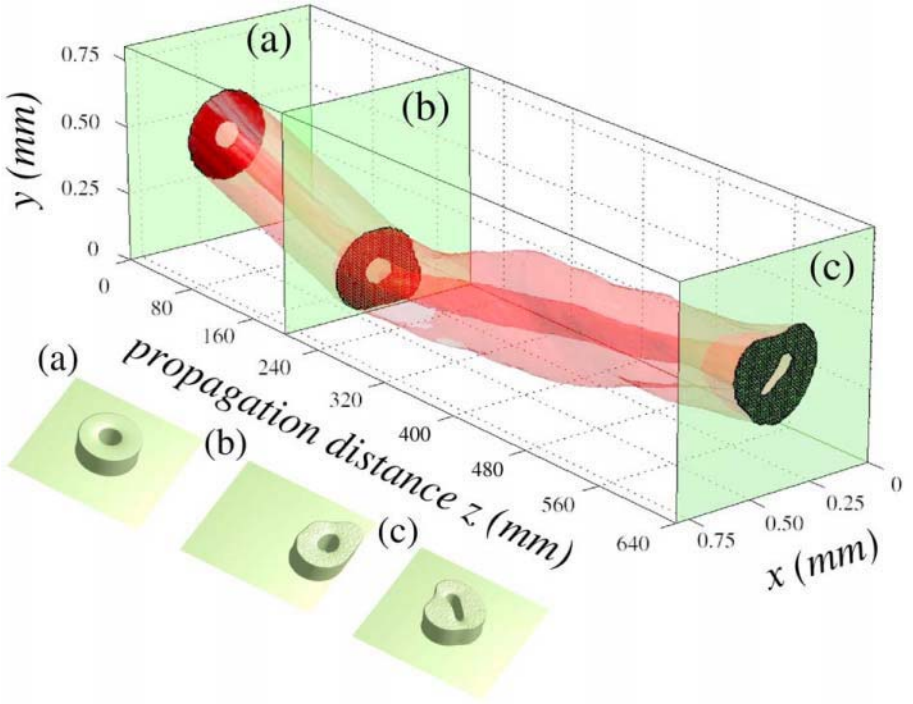

Figure 11. Numerical simulation of the total reflection at a planar boundary of an eigenstate with angular momentum l =4 and $\beta = 0.95\beta_{cr}$. The top image is the isosurface of the beam trayectory. The boundary between the nonlinear material and air is the plane $y = 0$. The images (a)-(c) correspond to intensity profiles of the beam cross section at different points.

momentum, including such high momentum cases as $l = 10$ and $l = 50$. As it is appreciated in these plots, there exists a window between the vanishing point and the limit value for β ($\beta = \beta_{cr}$) which proves the existence of a stability zone close to the critical point. This window narrows for high values of l but it remains finite. As l increases, the point at which the perturbation vanishes tends asymptotically to a value below the critical point. Therefore, whatever the value of l, there always exist a stability window containing an infinite number of stable eigenstates.

We have to stress that close to β_{cr} the azimuthal analysis turns itself very delicate and it has to be carried out in a careful way. In fact, convergence takes a much longer distance and an erroneous final result is obtained if the number of samples and the propagation step are not chosen appropriately. In this sense, combining the analysis with direct calculations of the splitting distance of the unstable eigenstates is definitively useful. In Fig. 10(d) it is zoomed the region of 10(c) where the

perturbation for $l = 3$ drops to zero. They are also plotted the points obtained propagating the eigenstates and taking the inverse of the distance where they split. These values were subsequently scaled by the same constant value to compare with the perturbation eigenvalue curve. It is appreciated that the values obtained from this propagation experiments fall to zero with the same slope as the perturbation eigenvalues do. When the stability analysis is not perform with enough accuracy a more steady behaviour of the curve appears, so that the eigenvalue falls to zero at a higher value of β. In this way, the validity of the perturbation analysis can be assessed.

As a final test of the stability of the eigenstates, we have simulated the total reflection at a planar boundary between a cubic-quintic material and air of beams with different angular momenta as it was done in section 5. For the simulation we have used a split-step Fourier method with a 512×512grid.

As it can be seen in Fig. 11, a beam with $l = 4$ does not split after the total reflection, although a strong oscillation is observed. This is another proof of the stability of these nonlinear waves. We must notice that depending on the incidence angle, a strong deformation of the beam can be induced, which can yield to a split or a decay of the inner vortex into several defects with lower charges.

10. Vortices in pulsed beams

Light whirpools can be induced in pulsed beams as well as in the continuous beams that we have previously studied. From the experimental point of view, it is more interesting to study the possibility of exciting these azimuthal beams starting with pulsed gaussian distributions under adequate conditions.

In Fig.12 we show the numerical simulation of the time evolution of two different light distributions propagating through an optical material with $n_0 = 1.8$, $n_2 = 2 \cdot 10^{-4} cm^2/GW$ and $n_4 = 0.8 \cdot 10^{-3} cm^4/GW^2$. The top-left image a) shows an initial condition consisting on three pulses (i.e.: light droplets) of $100\mu m$ diameter with $\lambda = 1.964nm$ and $I = 1.6GW/cm^2$ that are located at the vertices of a equilateral triangle. The beams are $2\pi/3$ out of phase. With this initial condition it can be seen that the pulses coalesce into a spiral structure b) which finally yields to the asymptotic rotating state c) with a nested vortex with topological charge $l = 1$. The second series of images d) to f) show the direct excitation inside a light droplet of a doubly-charged vortex, with two windings of the phase around the central hole. The experimental parameters are the same as in the previous case, despite the beam width is now $30\mu m$ and $I = 1.4GW$. The images have been rescaled for a better

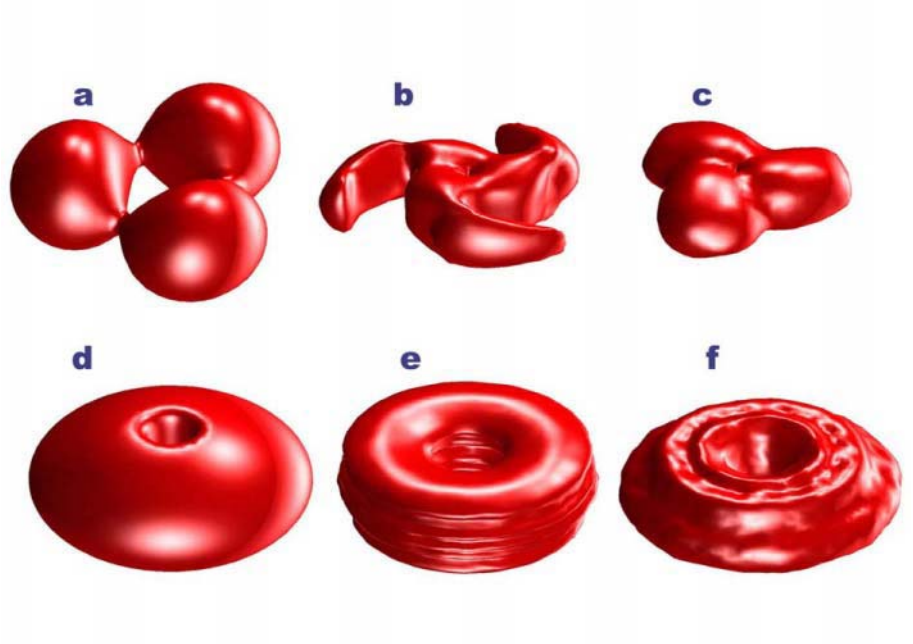

Figure 12. Top: the image a) shows an initial condition consisting on three pulses of $100\mu m$ diameter with $\lambda = 1.964nm$ located at the vertices of a equilateral triangle. The beams are $2\pi/3$ out of phase. The pulses coalesce into a spiral structure b) which finally yields to the asymptotic rotating state c) with a nested vortex with topological charge $l = 1$. Bottom: Evolution of the initial state d) consisting of a gaussian beam which is launched to a holographic phase mask with $l = 2$. After strong oscillations and formation of characteristic surface ripples in e), the beam tends to an asymptotic state with a nested "breathing hole" with topological charge $l = 2$, which is stable over many diffractive lengths. In both examples the material parameters and intensities are the same as for the continuous case.

ilustration. The azimuthal phase can be experimentally implemented with an adequate phase mask. As it can be seen, after strong oscillations and formation of characteristic surface ripples in e), the beam tends to an asymptotic state with a nested "breathing hole" with topological charge $l = 2$, which is stable over many diffractive lengths.

11. Conclusions

We have described the phenomenon of light condensation in nonlinear optical materials with cubic-quintic (C-Q) nonlinearity. To support the analogy between light condensates and quantum liquids, we have tested the surface tension properties of "light streams" and "light drops" by simulating collisions against planar boundaries and localized inhomo-

geneities. We have also shown the existence of a new kind of physical objects: stable azimuthal finite-size beams with arbitrary (integer) angular momentum that can exist in C-Q nonlinear optical materials. The shapes of these beams tend asymptotically to square-like ring profiles with bigger dark holes for higher values of the angular momentum. The critical values of the propagation constant and amplitude do not depend on the angular momentum of the beam. We have also studied the excitation of vortex states in this kind of nonlinear optical materials starting from gaussian beams with an adequate phase distribution. Our predictions open interesting questions about the nature and properties of what we have named "liquid light": a new state of matter-energy formed by nonlinear waves.

Acknowledgments

H. Michinel is partially supported by Ministerio de Ciencia y Tecnologia under grant TIC-2000-1105-C03-01.

References

[1] J. Stachel,(1998) *Einstein's miraculous year: five papers that changed the face of Physics,* Princeton University Press, Princeton.

[2] A. W. Snyder and D. J. Mitchell, "Accesible solitons", Science **276**, 1538-1547 (1997).

[3] G. I. Stegeman and M. Segev, "Optical spatial solitons and their interactions: universality and diversity", Science **286**, 1518-1521 (1999).

[4] *Optical Solitons: Theoretical Challenges and Industrial Perspectives,* edited by V. E. Zakharov and S. Wabnitz (1999). Springer Verlag, Berlin.

[5] *Wave Collapse*, edited by E. Kutnetsov, A. Zakharov, and E. Vladimir (1999) World Scientific, Singapore.

[6] C. Sulem and P. L. Sulem.(1999) *The Nonlinear Schrdinger Equation: Self-Focusing and Wave Collapse*, Springer Verlag, Berlin.

[7] Y. Silberberg, "Collapse of optical pulses", Opt. Lett. **15**, 1282-1285 (1990).

[8] N. N. Akhmediev, D. R. Heatley, G. I. Stegeman, and E. M. Wright, "Pseudorecurrence in two-dimensional modulation instability with a saturable self-focusing nonlinearity", Phys. Rev. Lett **65**, 1423-1426 (1990).

[9] A. H. Piekara, J. S. Moore, and M. S. Feld, "Analysis of self-trapping using the wave equation with high-order nonlinear electric permitivity", Phys. Rev. A **9**, 1403-1407 (1974).

[10] D. E. Edmundson and R. H. Enns, Phys. Rev. A **51**, 2491 (1995).

[11] C. Josserand and S. Rica, "Coalescence and droplets in the subcritical nonlinear Schrdinger equation", Phys. Rev. Lett. **78**, 1215-1218 (1997).

[12] R. McLeod, K. Wagner, and S. Blair, "(3+1)-dimensional optical soliton dragging logic", Phys. Rev. A **52**, 3254-3278 (1995).

[13] Z. Jovanoski, "Light bullet formation in a cubic-quintic nonlinear medium", J. Mod. Opt. **48**, 865-875

[14] F. Smektala, C. Quemard, V. Couderc, and A. Barthelemy, "Non-linear optical properties of chalcogenide glasses measured by Z-scan", J. Non-Cryst. Sol. **274**, 232-237 (2000).

[15] M. Quiroga-Teixeiro and H. Michinel, "Stable azymuthal stationary state in quintic nonlinear optical media", J. Opt. Soc. Am. B **14**, 2004-2009 (1997).

[16] M. Quiroga-Teixeiro, A. Berntson, and H. Michinel, "Internal dynamics of nonlinear beams in their groun states: short and long-lived excitation", J. Opt. Soc. Am. B **16**, 1697-1704 (1999).

[17] K. Dimitrievski, E. Reimhult, E. Svensson, A. hgren, D. Anderson, A. Berntson, M. Lisak, and M. L. Quiroga-Teixeiro, "Analysis of stable self-trapping of laser beams in cubic-quintic nonlinear media", Phys. Lett. A **248**, 369-376 (1998).

[18] V. I. Bespalov and V. I. Talanov, "Filamentary structure of light beams in nonlinear liquids"ZhETF Pis'ma **3**, 471-476 (1966).

[19] A. J. Campillo, S. L. Shapiro, and B. R. Suydam "Periodic breakup of optical beams due to self-focusing", Phys. Rev. Lett **23**,628-630 (1973).

[20] N. B. Abraham and W. J. Firth, "Overview of transverse effects in nonlinear-optical systems", J. Opt. Soc. Am. B **7**, 951-62 (1990).

[21] A. Gammal, T. Frederico, L. Tomio, and P. Chomaz, "Liquid-gas phase transition in Bose-Einstein condensates with time evolution", Phys. Rev. A **61**, 1602-1606 (2000)

[22] J. F. Nye and M. V. Berry, Proc. R. Soc. London A **336,** 165-190 (1974).

[23] D. Rozas, Z. S. Sacks, Jr G. Swartzlander *Phys. Rev. Lett.* **79**, 3399 (1997).

[24] L. Pismen, *Vortices in nonlinear fields*, (Oxford University Press, London, 1999).

[25] N. R. Heckenberg, R. McDuff, C. P. Smith, and A. G. White, Opt. Lett. **17**, 221-223 (1992).

[26] G. Indebetouw, J. Mod. Optics **40** 73 (1993).

[27] N. B. Baranova, B. Ya. Zel'dovich, A. V. Mamaev, N. F. Pilipetslii, and V. V. Shkukov, Pis'ma Zh. Eksp. Teor. Fiz. **33**, 206-209 (1981) [JETP Lett. **33**, 195 (1981)].

[28] N. B. Baranova, A. V. Mamaev, N. P. Pilipetskii, V. V. Shkukov, and B. Ya. Zel'dovich, J. Opt. Soc. Am. **73**, 525-528 (1983).

[29] N. B. Simpson, K. Dholakia, L. Allen, and M. J. Padgett, Opt. Lett **22**, 52-54 (1997).

[30] K. T. Gahagan and G. A. Swartzlander, Jr. , Opt. Lett. **21**, 827 (1996).

[31] C. O. Weiss, M. Vaupel, K. Staliunas, G. Slekys, and V. B Taranenko, Appl. Phys. B **68**, 151-168 (1999).

[32] J. Scheuer and M. Orenstein, Science **285**, 230-233 (1999).

[33] A. Mair, A. Vaziri, G. Weihs and A. Zeilinger, Nature **412**, 313-316 (2001).

[34] Yu. S. Kivshar and E. Ostrovskaia, Opt. Photon. News **12**, 24-28 (2001).

[35] V. I. Kruglov and V. M. Volkov, Phys. Lett. A **111**, 401-404 (1985).

[36] W. J. Firth and A. J. Scroggie 1996 *Phys. Rev. Lett.* **76** 1623.

[37] G. A. Swartzlander, Jr. and C. T. Law, Phys. Rev. Lett. **69**, 2503-2506 (1992).

[38] D. Mihalache, D. Mazilu, L.-C. Crasovan, I. Towers, A. V. Buryak, B. A. Malomed, L. Torner, J. P. Torres and F. Lederer, Phys. Rev. Lett. **88**, 073902-1-4 (2002).

[39] V. Tikhonenko and N. Akhmediev, Opt. Commun. **126**, 108-112 (1996).

[40] G. Fang, Y. Mo, Y. Song, Y. Wang, C. Li, and L. Song, Opt. Commun. **205**, 337-341 (2002).

[41] H. Michinel, J. Campo-Taboas, R. Garcia-Fernandez, J. R. Salgueiro, and M. Quiroga-Teixeiro, Phys. Rev. E **65**, 066604-1-7 (2002).

[42] D. Anderson, "Variational approach to nonlinear pulse propagation in optical fibers", Phys. Rev. A **27**, 3135 (1983).

[43] J. M. Soto-Crespo, D. R. Heatley, E. M. Wright, and N. N. Akhmediev, "Stability of the higher-bound states in a saturable self-focusing medium", Phys. Rev. A **44**, 636-644 (1991).